Computational fluid dynamic model of a tapered Holweck vacuum pump operating in the viscous and transition regimes. I. Vacuum performance

S. Giors[a)]
Varian S.p.A., 10040 Leinì, Torino, Italy and Dipartimento di Energetica, Politecnico di Torino, I-10129 Torino, Italy

E. Colombo and F. Inzoli
Dipartimento di Energetica, Politecnico di Milano, I-20133 Milano, Italy

F. Subba and R. Zanino
Dipartimento di Energetica, Politecnico di Torino, I-10129 Torino, Italy

(Received 3 May 2005; accepted 23 January 2006; published 23 June 2006)

Holweck molecular drag pumps are used as high-pressure stages in hybrid turbomolecular vacuum pumps, where they can operate in the transition and the viscous regime. In this article we develop a Navier-Stokes model of a Holweck pump with tapered pumping channels, applying slip-flow boundary conditions, to predict vacuum performances with and without gas flow. The commercial computational fluid dynamic code FLUENT is used to solve the model equations and to predict the pressure profile along the grooves. A specifically designed experiment is presented, whose arrangement provides the boundary conditions as input to the model and whose results are used to validate it. © *2006 American Vacuum Society.* [DOI: 10.1116/1.2178362]

I. INTRODUCTION

Holweck molecular drag pumps are used as high-pressure stages in hybrid turbomolecular vacuum pumps, where they are often specifically designed to operate in the viscous regime. In fact, the main benefit of drag stages is to unload turbomolecular stages, keeping them in molecular flow conditions (about 0.1 mbar range, where they can supply their best compression performances) when an outlet pressure up to about 20 mbars determines viscous flow conditions at the pump outlet.

The recent years have seen a large increase in the application of sophisticated mathematical models and simulation tools in the field of rarefied gas dynamics dealing with vacuum pumps and systems.[1–5] The most common computational techniques applied in this field are direct simulation Monte Carlo[6] (DSMC) and computational fluid dynamics (CFD).[7] The CFD technique has the practical advantage, above the others, that there are many well-established commercial codes available, which can cope with the complex three-dimensional (3D) geometry typical of vacuum pumps, but it also has the disadvantage that the hydrodynamic approach is not suitable for the highly rarefied regime. Quite obviously, the pump manufacturers see in these tools the possibility to further optimize their products and to reduce the prototype cost and time, replacing the actual experiments with numerical ones, once the tool is suitably validated. However, it should be noted that there are also some aspects of vacuum pump physics which are not yet well understood. Basically no work was done, e.g., in the field of heat exchange phenomena in turbomolecular and molecular drag pumps, which is a matter of high interest in recent high-gas-load industrial applications of these pumps.

The most relevant model of a Holweck pump is due to Sawada and Sugiyama,[8] who built a one-dimensional model starting form 3D Navier-Stokes (NS) equations and simplified them to a one-dimensional equation, providing good results and throwing some light on the Holweck pump mechanism.

The CFD study of a Holweck pump was carried out by Boulon and Mathes,[9] using a three-dimensional no-slip NS model. They showed a good agreement with the experimental data in the viscous regime, but they suggested the need of slip-flow boundary conditions to improve the accuracy when the Knudsen number based on the channel depth h, $\mathrm{Kn} \equiv \lambda/h$, where λ is the gas mean free path, became >0.01. Here their model's agreement became worse.

More recently, the Holweck pump was studied by Sharipov *et al.*,[10] using a kinetic approach based on the solution of the linearized BGK model Boltzmann equation. They neglected the pump's curvature and end effects. Their approach was quasi-three-dimensional because their computational process consisted of a sequential solution of four two-dimensional subproblems (longitudinal and transversal, Couette and Poiseuille flow) solved once and for all on the channel constant cross section, followed by the application of mass conservation to derive a one-dimensional equation for the pressure in the third longitudinal dimension. Similar to the slip flow NS model derivation from the Boltzmann equation, the kinetic model of Sharipov *et al.* is based on the assumption of a small perturbation with respect to the Maxwellian equilibrium distribution, but their validation does not show relevant Kn limitations.

a)Electronic mail: silvio.giors@varianinc.com

Although their approach was very computationally efficient due to the separation of the two-dimensional (2D) and one-dimensional (1D) solutions, it could become inapplicable or at least less efficient in case a tapered pump (with channel depth h variable between inlet and outlet) is analyzed. Furthermore, Sharipov *et al.* claim in the conclusions of their work that "at the pressures of Holweck pump functioning the gas rarefaction is [a] predominant factor, i.e., the Navier-Stokes equation is not appropriate for the modeling of such a pump even if one uses the slip boundary condition." On the contrary, we will show here that such a model is able to accurately reproduce the measured results in a relatively broad range of Kn already of interest in the applications, particularly when a relatively high mass flow rate of gas is pumped. Note that a similar conclusion on the applicability and value of the slip-flow boundary conditions to the NS equations was already demonstrated by Giors *et al.*[11] in the application to a Gaede drag pump.

In this article the emphasis is on the application of the NS equations with slip-flow boundary conditions to a three-dimensional model of a single-stage tapered Holweck pump, i.e., a Holweck pump with tapered pumping channels going round the periphery of the rotor only once (about 180°) to predict vacuum performances. Thermal aspects will be presented in a companion article. The three-dimensional NS approach, in spite of the recognized limitations at high Kn, was chosen to derive accurate results in a tapered 3D geometry and in cases of high throughput, typical of a recent industrial application of these devices.

To be able to model the pump correctly, some boundary conditions must be provided as input. For this reason and to validate the model results, an experiment was designed and is also described here.

The article is organized as follows. Section II describes the experiment. Section III describes the model equations and boundary conditions. Section IV shows the results and interprets them in terms of previous theories. In Sec. V some conclusions and future work perspectives are discussed.

II. EXPERIMENTAL SETUP

The tested single-stage Holweck pump is made of a smooth cylindrical rotor rotating inside a stator, where 14 linearly tapered parallel grooves are machined in the wall. The geometry of the pump and its modeling relevant dimensions are represented in Fig. 1.

A. Experimental apparatus

An experiment was designed to validate the model. It also provided some input parameters necessary to solve it. The measured outlet pressure, mass flow rate, and rotor and stator temperatures are imposed as input boundary conditions, while the inlet pressure and the pressure profile along the channel are the main model output. The test was performed with nitrogen (N_2). The experimental apparatus is represented in Fig. 2. An asynchronous motor drives the rotor at a rotation frequency $f_{\text{rotor}}=928$ Hz$\pm 1\%$ (variation due to the slip at variable load).

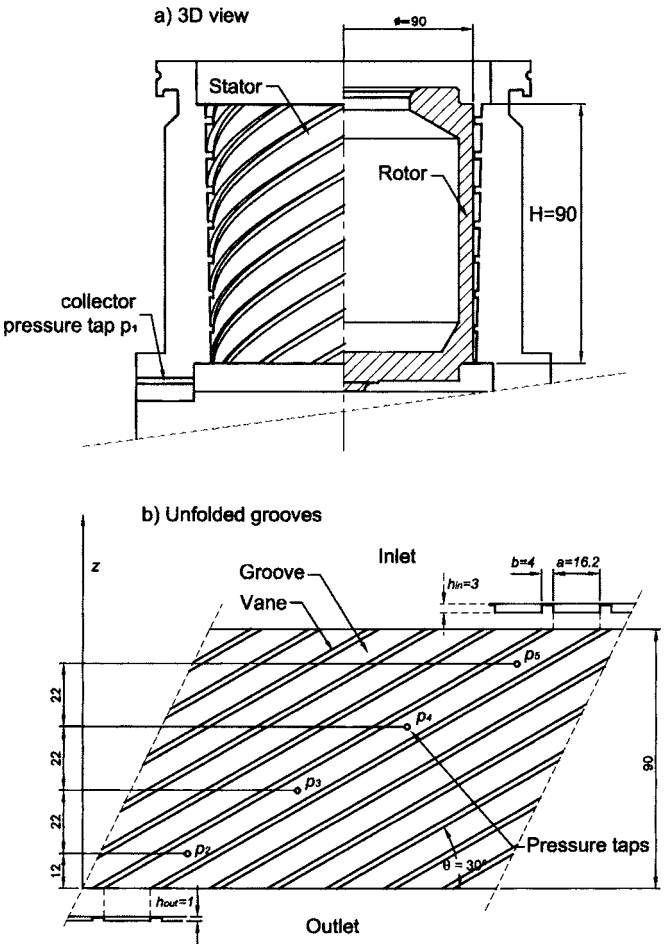

FIG. 1. Sketch of the Holweck pump and pressure taps location (dimension in millimeters): (a) 3D view of rotor and stator and (b) 2D unrolled stator representation.

The nonlinear pressure profile is measured using six capacitance absolute pressure gauges: one (p_1) positioned on the outlet collector, four (p_2–p_5) along one helical groove, and one (p_6) in the inlet vacuum chamber (test dome according to ISO-5302). The location of the five pressure taps along a pump groove can be seen in Fig. 1. The mass flow rate entering the vacuum chamber, $\dot{m}_{\text{in}}$, is set and measured by a mass flow controller. Stator and rotor temperatures are measured by two thermocouples (T_1 and T_2) and an infrared (IR) camera (T_{rotor}), respectively. The two thermocouples, placed in two axial positions on the pump stator, measured temperature differences <5 K. The IR camera could see the high vacuum side of the rotor through an IR transparent window placed on top of the vacuum chamber, and it showed an almost uniform T_{rotor}.

The f_{rotor} is measured by an inductive proximity sensor and a frequency counter, reading the passage of a notch on the rotor surface. The measured parameters, the instrumentation, and the measurement accuracy are listed in Table I.

Two kinds of tests are carried out:

- Zero gas flow test, in which $\dot{m}_{\text{in}}=0$ (outgassing is assumed to be insignificant in the considered pressure range); and

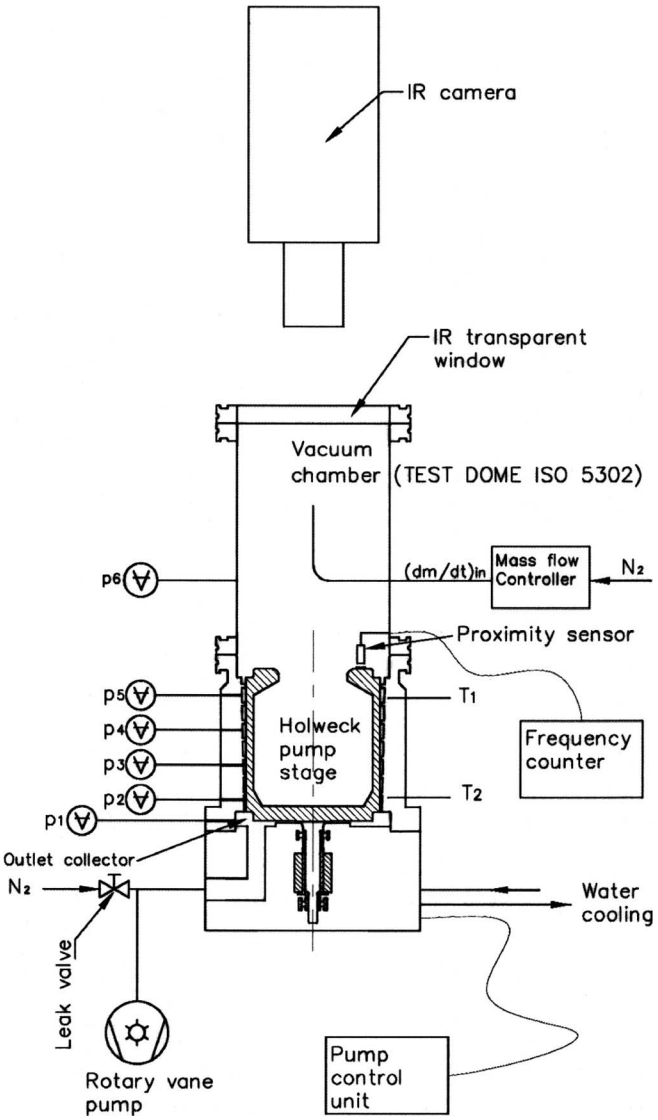

FIG. 2. Sketch of the experimental setup.

- Constant throughput test, in which $\dot{m}_{in}=250$ SCCM (standard cubic centimeter per minute) ($cm^3 \times min^{-1}$ at 760 torr and 273.15 K), set by the mass flow controller.

In both tests the pressure profile along the groove is measured for several values of p_1 by tuning a leak valve on the outlet of the pump, and the measurement is performed after checking that the thermal and mechanical equilibria have been reached.

B. Operating conditions and corresponding flow regime

The pump is tested in the following pressure range: 0.7 mbar $\leqslant p_1 \leqslant$ 20 mbars and 6×10^{-5} mbars $\leqslant p_6 \leqslant$ 10 mbars. The flow regime can be defined by a set of nondimensional parameters. The maximum Reynolds and Mach numbers are defined as $\mathrm{Re}\equiv\rho_{out}Vh_{out}/\mu\cong350$ and $M\equiv V/\sqrt{\gamma R^* T}\cong0.72$. They are estimated using the rotor peripheral speed $V\cong260$ m/s as representative of the gas velocity at $T=300$ K, $p_6=20$ mbars, $\rho_{out}=p_6/R^*T$, $\gamma=1.4$, $R^*=R/m$, $R=8.314$ J K^{-1} mol^{-1}, $m=28.01$ kg $kmol^{-1}$. The gas rarefaction can be evaluated by Kn, which spans a very large interval in our experiment due to the different tested operating conditions and to the pressure variation along the pump: $4\times10^{-3}<\mathrm{Kn}<500$, implicates that the range evolves from viscous to molecular.

TABLE I. List of the instrumentation used and corresponding measurement accuracy.

Measured quantity	Instrumentation	Measurement accuracy
p_1–p_6	MKS Baratron® diaphragm absolute pressure gauges, 0.1, 10, 100 mbar full scale	±5% of reading
$\dot{m}_{in}$	MKS mass flow controller, 1000 SCCM full scale	±3% of reading
T_1 T_2	*K*-type thermocouples	±1 K
T_{rotor}	FLIR SC-500 infrared camera	±2 K
f_{rotor}	Contrinex NAMUR proximity sensor and HP 3584A frequency counter	±0.5 Hz

III. MODELING

A. Mathematical model

According to the estimations of Kn, Re, and *M* cited in the previous section, the model is based on laminar and compressible Navier-Stokes equations, including the energy equation and the viscous heating as well as applying slip-flow boundary conditions at the walls (see below). The ideal-gas law is used as an equation of state for nitrogen: $p=\rho R^* T$. Even if the gas temperature variation in the domain is not large compared to the absolute average temperature, we enable the gas transport properties to vary with temperature (variation of about 10%) because this improves the model accuracy without increasing its computational cost. We use Sutherland's law for the viscosity μ and a polynomial law for the thermal conductivity k (see Table II).

As far as the slip-flow boundary conditions are concerned, we use a simplified formulation, neglecting the thermal creep term:[11]

$$u_{\tau,\mathrm{gas}} - u_{\tau,\mathrm{wall}} = \sigma_P \lambda \frac{\partial u_{\tau,\mathrm{gas}}}{\partial n}, \tag{1}$$

TABLE II. Nitrogen properties vs absolute temperature *T*: Sutherland's law for viscosity, $\mu=\mu_0(T/T_0)^{3/2}(T_0+S)/(T+S)$; polynomial law for thermal conductivity, $k(T)=A_1+A_2T+A_3T^2$.

	μ_0	T_0	S
μ	$1.663\ 10^{-5}$ Pa s	273.11 K	106.67 K
	A_1	A_2	A_3
k	$4.737\ 10^{-3}$ W/m/K	$7.272\ 10^{-5}$ W/m/K^2	$-1.122\ 10^{-8}$ W/m/K^3

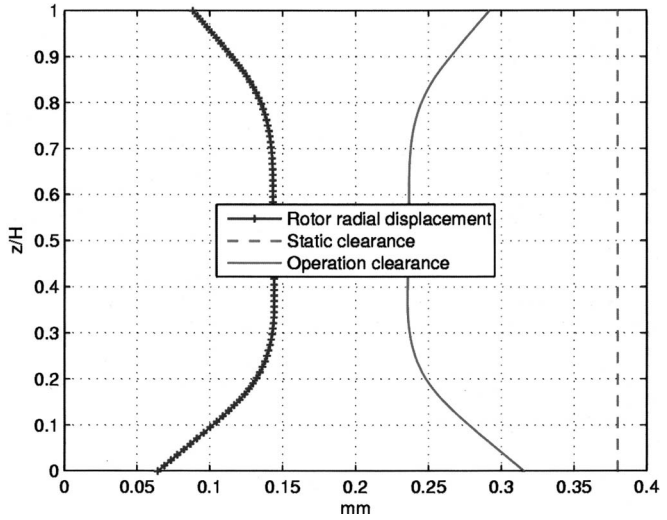

FIG. 3. Rotor deformation from the FEM model and its effect on the clearance between rotor and stator.

$$T_{\text{gas}} - T_{\text{wall}} = \varsigma_T \lambda \frac{\partial T_{\text{gas}}}{\partial n}. \tag{2}$$

Equations (1) and (2) state that there is a difference between the macroscopic tangential component of the gas velocity $u_{\tau,\text{gas}}$ close to the wall and the wall velocity $u_{\tau,\text{wall}}$ (velocity slip), as well as between the gas temperature T_{gas} close to the wall and the wall temperature T_{wall} (temperature jump). These differences are related to the normal $(\partial/\partial n)$ gradient of the bulk gas velocity and temperature through the viscous slip (σ_p) and thermal jump (ς_T) coefficients. The latter are expressed in terms of the momentum (α_t) and energy (α_n) accommodation coefficients:

$$\sigma_P = \frac{2-\alpha_t}{\alpha_t}; \quad \varsigma_T = 2\frac{2-\alpha_n}{\alpha_n}. \tag{3}$$

The expression used in our computation for the parameter λ in Eqs. (1) and (2) is based on the Lennard-Jones characteristic length for nitrogen $\delta = 3.621$ Å: $\lambda = k_B T/\sqrt{2}\pi\delta^2 p$, where T and p are the gas local temperature and pressure, respectively, and k_B is the Boltzmann constant. Based on Giors *et al.*[11] in this work we use $\alpha_t = \alpha_n = 0.91$, which gives $\sigma_P = 1.19$ and $\varsigma_T = 2.39$.

B. Computational domain and boundary conditions

The computational domain is built using the geometrical dimensions of the tested pump, measured with a ±0.01 mm accuracy. In addition, the rotor wall profile is built, accounting for the radial deformations due to centrifugal forces (about 0.1 mm) and thermal expansion (about 0.04 mm due to a temperature difference between rotor and stator of about 40 K), obtained by a finite element method (FEM) calculation. These effects reduce the clearance between the rotor and the stator vane's tip, e, from the static value of 0.38 mm to the profile in operation, variable between about 0.24 and 0.32 mm (shown in Fig. 3). Indeed, sensitivity calculations carried out repeating the simulations with different values of a uniform clearance, in the interval [0.24, 0.38 mm], showed that the calculated pressures are sensitive, outside the experimental uncertainty, to a variation of the clearance of a few hundredths of millimeters.

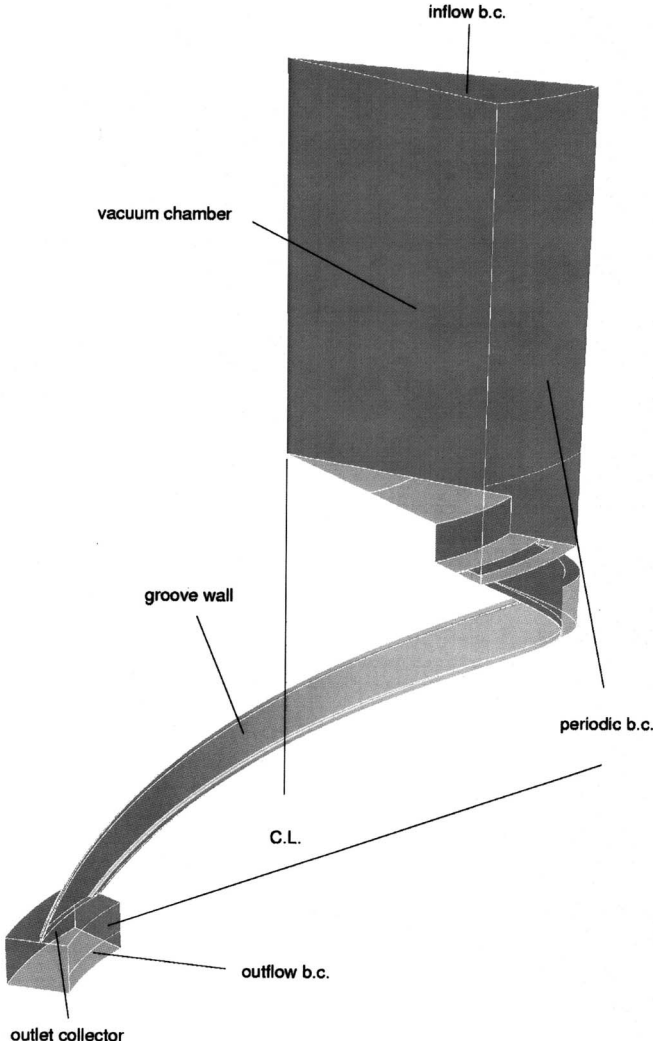

FIG. 4. Periodic computational domain used to model the Holweck pump.

The computational domain is represented in Fig. 4. Taking advantage of the periodic geometry of the stator (14 grooves in parallel), the domain is limited to one groove, bounded by half a vane at both sides. Periodic boundary conditions are imposed at the cuts. In order to represent correctly the phenomena occurring at the entrance and at the exhaust of the groove, a 360°/14 wide cylindrical sector of the low-pressure vacuum chamber and of the high-pressure outlet collector are added to the pumping groove. This also allowed the imposing of the inlet and outlet boundary conditions in compliance with the experimental setup.

At the inflow boundary the gas temperature (assumed in equilibrium with the measured temperature of the vacuum chamber) and the measured $\dot{m}_{\text{in}}$ are imposed, at the outflow boundary the measured outlet pressure, $p_{\text{out}} = p_1$, is imposed.

At the walls (rotor, stator, and vacuum chamber) slip flow and thermal jump boundary conditions are imposed. Wall

temperatures $T_{stator}=(T_1+T_2)/2$ and T_{rotor}, and rotor tangential velocity $u_{\tau,wall}=2\pi f_{rotor}r$, where r is rotor's radius, are measured from the experiment and used in the boundary conditions.

C. Numerical solution

The finite volume method[7] is used to discretize the NS equations. The computational domain is first subdivided into about 6×10^5 hexahedral control volumes, constituting a nonuniform, block structured, boundary fitted grid. The grid edges are well aligned with the walls and the main flow velocity in order to reduce the numerical viscosity, i.e., a false viscosity coming out of the discretization process.[7] Two details of the surface mesh, at the inlet and outlet of the groove, are represented in Fig. 5. This particular mesh was used to obtain the results presented below.

The numerical solution is carried out with the commercial code FLUENT,[12] using second order upwind discretization schemes for convective fluxes.[7] The segregated solver (SIMPLE algorithm[7]) is used to linearize the system of equations. The main output of the computation is the average pressure in the vacuum chamber, p_{in}. The grid sensitivity of the solutions was verified repeating the calculations on a refined grid, with about 1.4×10^6 control volumes. The difference on p_{in} was $\leqslant3\%$.

IV. RESULTS

Both experiments, zero gas flow and 250 SCCM constant throughput flow, were simulated. The global results are represented in Fig. 6 in a nondimensional form. The inlet rarefaction parameter $\delta_{in}=p_{in}h_{in}/\mu\nu_0=1/\mathrm{Kn}_{in}$ is plotted versus the outlet rarefaction parameter $\delta_{out}=p_{out}h_{out}/\mu\nu_0=1/\mathrm{Kn}_{out}$, where $\nu_0=\sqrt{2R^*T}$ is the most probable molecular velocity at $T=300$ K.

Figure 6(a) shows the validation with the zero gas flow of both our slip-flow and no-slip versions of our model, implemented imposing zero velocity slip and temperature jump at the walls. The agreement between the slip-flow model and the experiment is very good for $\delta_{out}\geqslant120$, which corresponds to $p_{out}\geqslant9$ mbars and $\mathrm{Kn}_{in}=1/\delta_{in}<0.12$. At lower pressures the agreement becomes progressively worse due to the fact that the flow regime is becoming molecular at the inlet of the pump, where $\mathrm{Kn}_{in}>0.1$. The model with no-slip boundary conditions shows a good agreement only for pressures corresponding to $\mathrm{Kn}_{in}=1/\delta_{in}<0.01$. Hence it can be claimed that slip-flow boundary conditions extend the accuracy of the NS model of the Holweck pump towards higher Kn to one decade. This result agrees with the results by Giors *et al.*[11] for a Gaede vacuum pump, and also with the generally accepted limit of validity of the NS model with slip-flow boundary conditions, i.e., $\mathrm{Kn}=0.1$.[13] Based on this, only the slip-flow model results will be reported below.

Figure 6(b) shows the validation with a 250 SCCM constant throughput flow. The agreement between the model and the experiment is very good (well within the experimental error bars) for the whole range of both δ_{in} and δ_{out}, which, in this experiment, are always greater than about 10. Figure 7 shows the same results as Fig. 6, expressed in terms of pressure difference $\Delta p=p_{out}-p_{in}$ vs p_{out} [Fig. 7(a)] and pumping speed $S=\dot{m}_{in}/p_{in}$ vs p_{out} [Fig. 7(b)]. At high pressure Δp as a function of p_{out} saturates to an almost constant value of about 10 mbars [Fig. 7(a)], in qualitative agreement with the approximate and optimistic solution of the one-dimensional model of drag pumps in the viscous regime.[14] $\Delta p\cong6\mu V/h_{in}h_{out}H/\tan(\theta)(1-\bar{e}/\bar{h})\cong12.5$ mbars, where $\bar{e}$, $\bar{h}$ are average values along z. Figures 6(b) and 7(b) shows that at low p_{out}, for a constant $\dot{m}_{in}$, p_{in} is limited by the pump's maximum pumping speed $S=\dot{m}_{in}/p_{in}\cong20$ l/s. This value is substantially lower than the approximate value,[15] $S\cong V/2\pi\phi h_{in}a/(a+b)\sin(\theta)\cos(\theta)(1-e_{in}/h_{in})\cong34.4$ l/s,

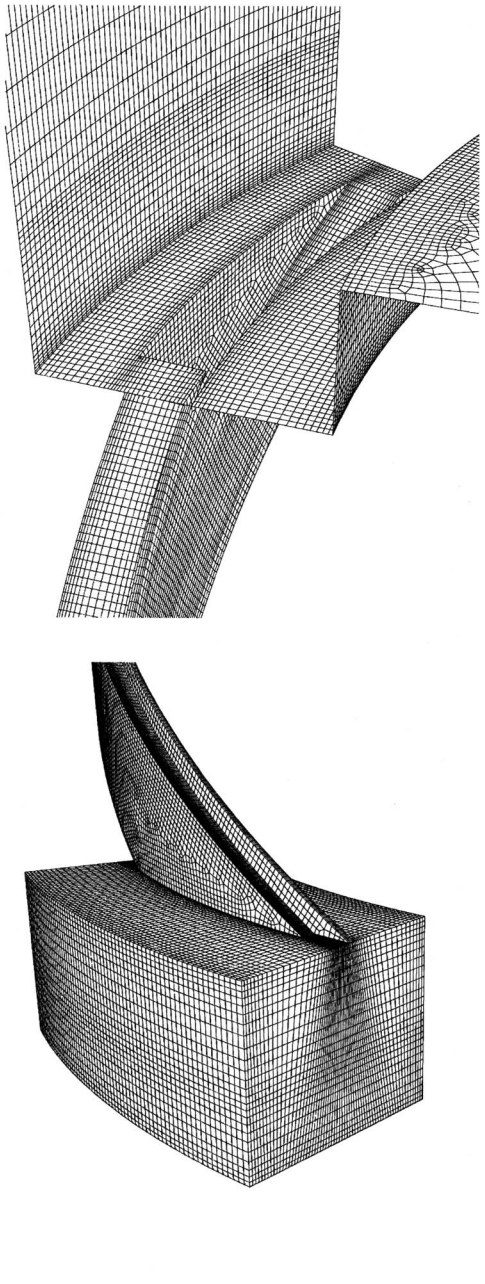

FIG. 5. Example of the computational mesh: (a) channel inlet detail and (b) channel outlet detail.

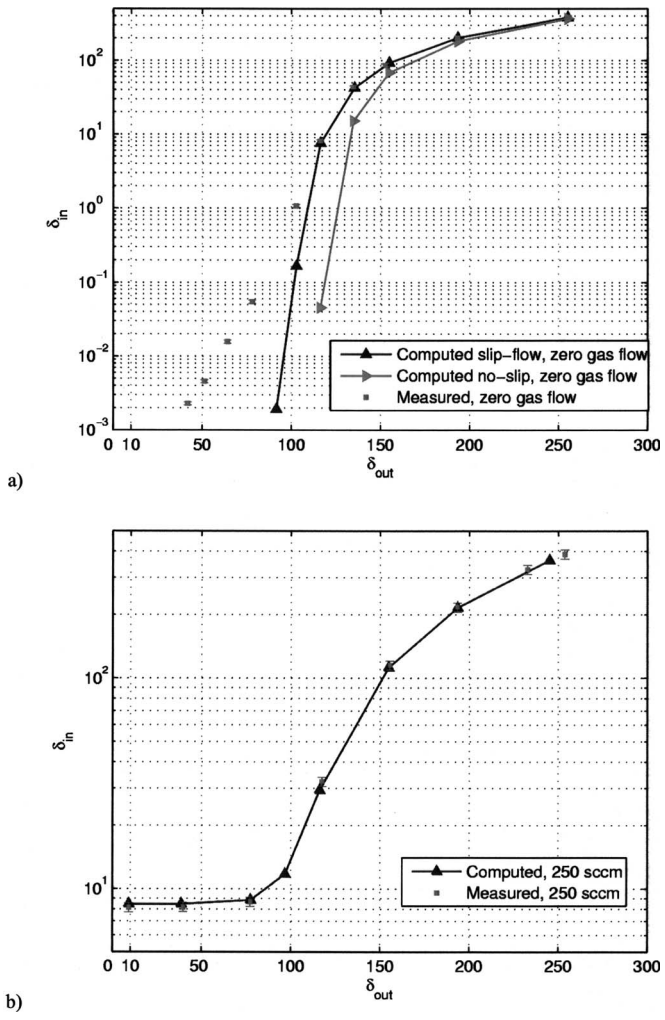

FIG. 6. Comparison of computed and measured inlet vs outlet rarefaction parameter: (a) zero gas flow and (b) constant throughput gas flow (250 SCCM).

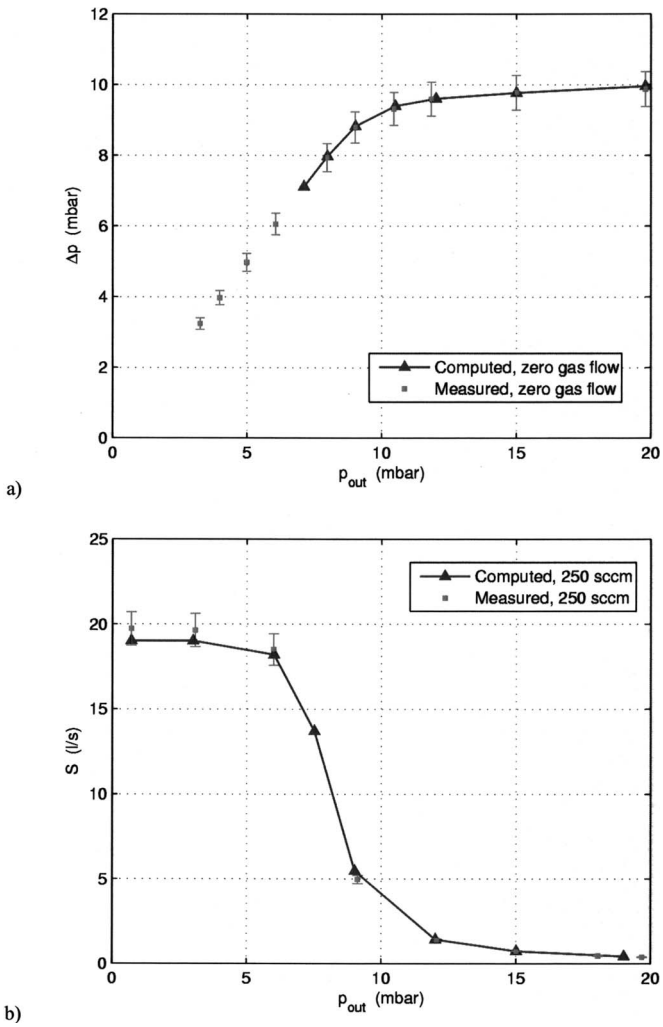

FIG. 7. (a) Pressure difference $\Delta p = p_{out} - p_{in}$, with zero gas flow, and (b) Pumping speed $S = \dot{m}_{in}/p_{in}$, with $\dot{m}_{in} = 250$ SCCM, both as functions of p_{out}.

which neglects the actual velocity distribution in the groove, the effect of the adverse pressure gradient arising in a tapered channel when $p_{out} \cong p_{in}$, and the entrance conductance effects. It is known[15] that a tapering ratio $h_{in}/h_{out} = 10$ can provide about ten times higher Δp, but up to 60% lower maximum speed than a pump with the same inlet cross section and other geometrical parameters, but uniform channels. Our model can provide a relevant accuracy improvement with respect to the available approximate theories, still maintaining a qualitative agreement with them.

Figure 8 shows the comparison between the pressure measurement in the six pressure taps along the pump, the computed pressures in the same locations, and the computed pressure profile along the channel centerline (the pressure taps were not exactly aligned with the groove centerline owing to a manufacturing error). The pressure taps and profile, distributed along a helical path, are here localized by their z position. Figure 8(a) refers to $p_{out} \cong 10.5$ mbars ($\delta_{out} \cong 150$) and the zero gas flow. Figure 8(b) refers to $p_{out} \cong 0.7$ mbar ($\delta_{out} \cong 10$) and $\dot{m}_{in} = 250$ SCCM. In both cases the agreement between measured and computed pressures is within the experimental uncertainty.

The computed profiles are nonlinear. This can be explained by the tapering of the grooves, which increases the pressure gradient from the inlet to the outlet: $dp/dz \propto 1/h(z)^2$.[8] Some nonmonotonic effects close to the groove entrance ($z=0$) and exit ($z=H$) are also shown. These are more marked in the $\dot{m}_{in} = 250$ SCCM case. In the latter case [Fig. 8(b)] there is a pressure drop in the streamwise direction, at the groove entrance and exit, which can be easily explained in terms of a localized Δp at the entrance of $\dot{m}_{in}$ into the channel from a large reservoir and out of the channel into the collector.

Figure 9 shows some local results. Figure 9(a) shows the contours of constant pressure on the surface of the rotor in the conditions where $p_{out} \approx 10.5$ mbars and $\dot{m}_{in} = 0$. The pressure contours are aligned with the cylindrical rotor axis in the center of the grooves. This agrees with Helmer's conjecture,[16] according to which the pressure gradient, at first order, has to be aligned with its tangential driving force,

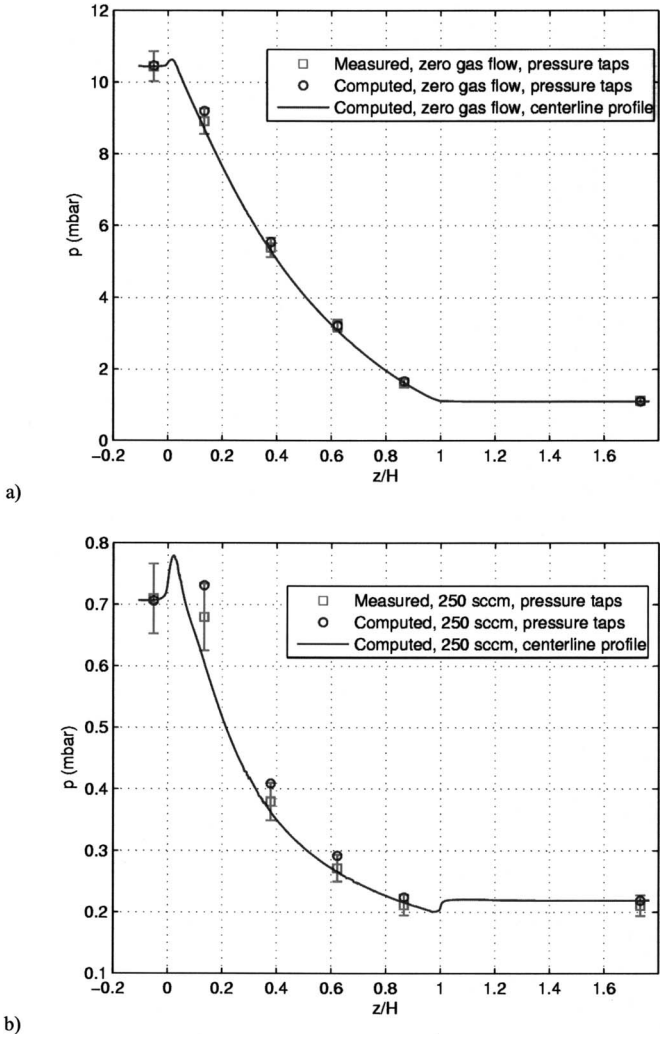

FIG. 8. Comparison of computed and measured pressure profiles along the pump: (a) zero gas flow ($p_{out} \cong 10.5$ mbars) and (b) constant throughput gas flow ($p_{out} \cong 0.7$ mbar, $\dot{m}_{out} = 250$ SCCM).

namely, the rotor's drag. This shape of the contours is broken by the presence of the groove separating vanes. This result is in disagreement with the modeling work of many authors,[8,10] who assume a constant pressure on the channel normal cross section, which is, quite obviously, never aligned with the rotor axis. The fact that they obtain good results anyway can be explained by the small channel width to length ratio of the pumps considered, but their models could fail for pumps in which this condition is not fulfilled.

Figure 9(b) shows the contours of a constant tangential velocity on a channel cross section at $z = 80$ mm. The gas flows forward (along the counterclockwise rotor drag direction) close to the rotor itself, and backward in the center of the groove, owing to the pressure gradient effect. This can be interpreted in the classical framework of Couette-Poiseuille theories for molecular drag pumps.[14]

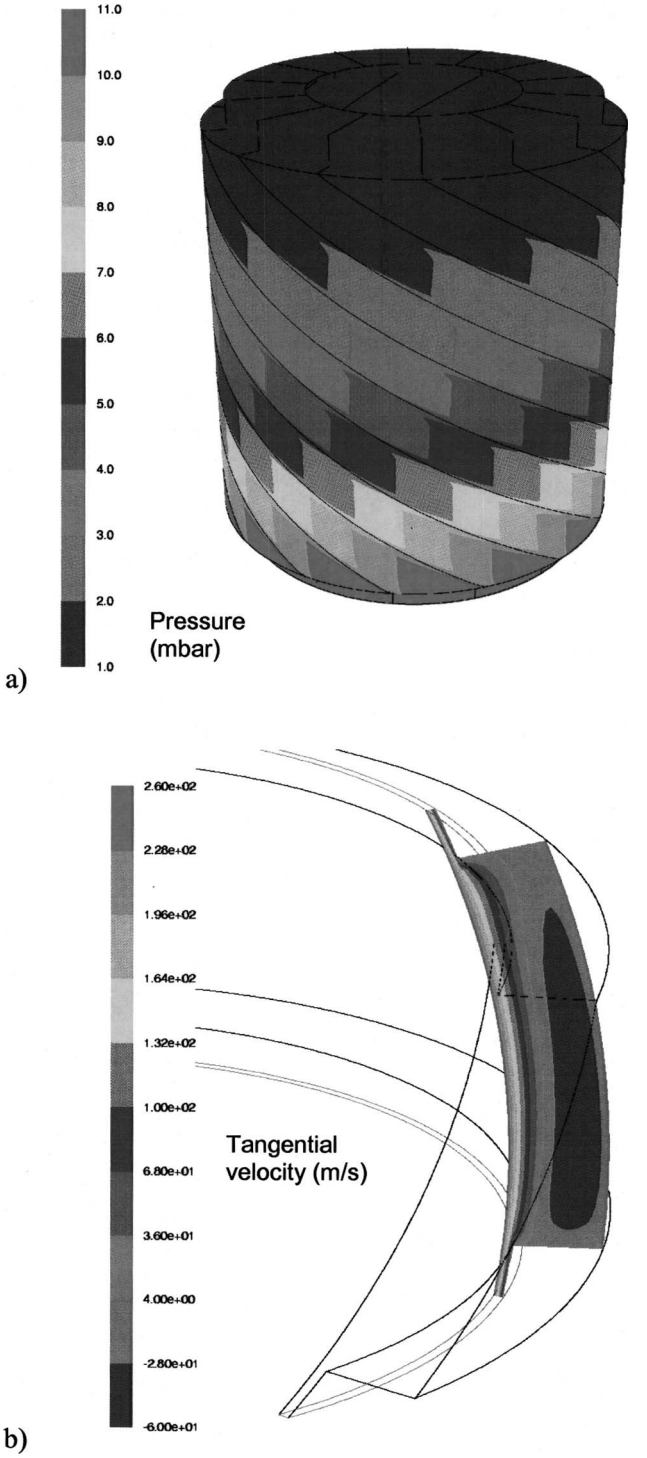

FIG. 9. Pressure and velocity fields at zero gas flow, $p_{out} \cong 10.5$ mbars: (a) contours of constant pressure (mbar) on the rotor surface and (b) contours of constant tangential velocity (m/s, positive counterclockwise) on a channel cross section at $z = 80$ mm.

V. CONCLUSIONS AND PERSPECTIVES

A Navier-Stokes model with slip-flow boundary conditions was developed for a Holweck pump with tapered channels to compute the pumping performances with and without gas flow. An experiment was built to provide input boundary conditions to the model and to validate it in terms of pressures measured in six locations along the pump. The validation shows a very good agreement in the pressure range corresponding to $Kn_{in} < 0.1$, namely, in the viscous part of the

transition flow regime (sometimes called slip-flow regime). The agreement here may be considered more than adequate for design purposes. The agreement becomes worse for higher Kn_{in}, as expected by the intrinsic limits of the hydrodynamic approach. At $Kn_{in} < 0.1$ the results show a significant quantitative improvement in accuracy compared to the presently available pure one-dimensional models and can also be qualitatively interpreted in terms of previous Couette-Poiseuille theories.

A future work will concentrate on heat exchange phenomena in order to predict the rotor's temperature. The wall temperatures, instead of being measured and imposed as boundary conditions, will be calculated self-consistently, coupling the heat flux at the fluid domain wall boundary to the heat conduction in the solid parts of the pump. This procedure will be presented in a forthcoming second part of this work.

ACKNOWLEDGMENTS

Varian S.p.A. supported this work. The authors wish to thank C. Quartarone for this support with the FEM calculation of the rotor deformation and J. C. Helmer for his stimulating review of the manuscript.

[1]H.-P. Cheng, R.-Y. Jou, F.-Z. Chen, Y.-W. Chang, M. Iwane, and T. Hanoka, Vacuum **53**, 227 (1999).
[2]H.-P. Cheng, R.-Y. Jou, F.-Z. Chen, and Y.-W. Chang, J. Vac. Sci. Technol. A **18**, 543 (2000).
[3]J.-S. Heo and Y.-K. Hwang, J. Vac. Sci. Technol. A **19**, 656 (2001).
[4]Y.-K. Hwang and J.-S. Heo, J. Vac. Sci. Technol. A **19**, 662 (2001).
[5]S. Giors and F. Subba, J. Vac. Sci. Technol. A **22**, 1828 (2004).
[6]A. Bird, *Molecular Gas Dynamics and the Direct Simulation of Gas Flows* (Oxford University Press, Oxford, 1994).
[7]J. H. Ferziger and M. Peric, *Computational Methods for Fluid Dynamics* (Springer, Berlin, 2002).
[8]T. Sawada and W. Sugiyama, J. Vac. Sci. Technol. A **17**, 2069 (1999).
[9]O. Boulon and R. Mathes, Vacuum **60**, 73 (2001).
[10]F. Sharipov, P. Fahrenbach, and A. Zipp, J. Vac. Sci. Technol. A **23**, 1331 (2005).
[11]S. Giors, F. Subba, and R. Zanino, J. Vac. Sci. Technol. A **23**, 336 (2005).
[12]*FLUENT 6.1 User's Guide* (Fluent, Lebanon Pennsylvania, 2003).
[13]A. Beskok and G. E. Karniadakis, J. Thermophys. Heat Transfer **8**, 647 (1994).
[14]M. Spagnol, R. Cerruti, and J. Helmer, J. Vac. Sci. Technol. A **16**, 1151 (1998).
[15]S. Giors, R. Gotta, and J. C. Helmer, Varian Vacuum Technologies Report No. RTMP02R001, 2002 (unpublished).
[16]J. C. Helmer (private communication).